行政院國家科學委員會專題研究計畫　成果報告

二極體雷射吸收光譜診測技術之研發及應用於努森壓縮熱電系統之量測

計畫類別：整合型計畫
計畫編號：NSC93-2212-E-216-004-
執行期間：93 年 08 月 01 日至 94 年 08 月 31 日
執行單位：中華大學機械與航太工程研究所

計畫主持人：鄭藏勝

計畫參與人員：趙怡欽 教授、吳志勇(博士後研究員)、張智國(博士生)、楊偉仁(碩士生)

報告類型：精簡報告
報告附件：出席國際會議研究心得報告及發表論文
處理方式：本計畫涉及專利或其他智慧財產權，1 年後可公開查詢

中　華　民　國 94 年 11 月 11 日

行政院國家科學委員會補助專題研究計畫 ■ 成 果 報 告 □期中進度報告

二極體雷射吸收光譜診測技術之研發及應用於努森壓縮熱電系統之量測
Development and Application of Diode Laser-Based Absorption Spectroscopy for Combustion Diagnostics in a Knudsen Compression Thermoelectric System

計畫類別：■ 個別型計畫　□ 整合型計畫
計畫編號：NSC　93－2212－E －216－004－
執行期間：　93 年　8　月　1 日至　94 年　8　月　31　日

計畫主持人：鄭藏勝 教授
共同主持人：
計畫參與人員：趙怡欽 教授、吳志勇(博士後研究員)、張智國(博士生)、楊偉仁(碩士生)

成果報告類型(依經費核定清單規定繳交)：■精簡報告　□完整報告

本成果報告包括以下應繳交之附件：
□赴國外出差或研習心得報告一份
□赴大陸地區出差或研習心得報告一份
■出席國際學術會議心得報告及發表之論文各一份
□國際合作研究計畫國外研究報告書一份

處理方式：除產學合作研究計畫、提升產業技術及人才培育研究計畫、列管計畫及下列情形者外，得立即公開查詢
□涉及專利或其他智慧財產權，□一年□二年後可公開查詢

執行單位：中華大學機械與航太工程研究所

中　華　民　國　94　年　11　月　30　日

行政院國家科學委員會九十三年度專題研究計畫成果報告

二極體雷射吸收光譜診測技術之研發及應用於努森壓縮熱電系統之量測
Development and Application of Diode Laser-Based Absorption Spectroscopy for Combustion Diagnostics in a Knudsen Compression Thermoelectric System

計畫編號: NSC 93-2212-E-216-004
執行期限: 93 年 8 月 1 日 至 94 年 8 月31 日
主持人:鄭藏勝 中華大學機械與航太工程研究所
E-mail: tscheng@chu.edu.tw

1. 摘要

本計畫「二極體雷射吸收光譜診測技術之研發及應用於努森壓縮熱電系統之量測」申請時為三年期整合型計畫之其中一子計畫，而計畫之目標在發展以二極體雷射為光源之吸收光譜診測技術，並希望以此技術量測努森壓縮熱電系統內之溫度及生成物濃度資訊，進而鑑定其對微反應系統性能之影響。但國科會核准本計畫為一年期之個別型計畫，因此本報告將針對以二極體雷射為光源之吸收光譜原理、碳氫燃料燃燒產物之近紅外光吸收譜線模擬、實驗架構原型設計與測試進行討論。

關鍵字：二極體雷射、吸收光譜、努森壓縮機、微動力及推進系統

2. Abstract

The objective of this research is to develop and apply diode laser-based absorption spectroscopy for combustion diagnostics in micro-electro-mechanical systems (MEMS) based Knudsen compression microscale power generation and propulsion systems. In this report, the theory of diode-laser based absorption spectroscopy, theoretical predictions of hydrocarbon fuel combustion products (CO_2, CO, O_2, H_2O, CH_4), and design and test of experimental setup will be discussed.

Keywords: Diode laser, Absorption spectroscopy, Knudsen compressor, Micro power generation and propulsion systems

3. Introduction

With increasing demands on micro devices such as micro- or pico-satellites and micro air vehicles (MAV), needs for a micro power source to activate these systems have been increased as well [1]. These systems require high energy density power source to provide a long period of time of operation. It is well known that the use of combustion processes for electrical power generation provides enormous advantages over batteries in terms of energy storage per unit mass and in terms of power generation per unit volume, even when the conversion efficiency in the combustion process from thermal energy to electrical energy is taken into account. Generally, the energy density of typical hydrocarbon fuels is about 100 times higher than that of batteries. Even regarding the heat losses in the process of extracting power from the fuel, a microcombustion device has been considered as a viable alternative to the batteries [2]. With the advances in microelectronics and micro electro-mechanical systems (MEMS), there is considerable interest in miniaturizing the propulsion and power systems as well. Various propulsion devices such as micro heat engine, gas turbine, rocket engine, and thruster have been successfully demonstrated [3, 4].

Along the development of micro reacting systems, existing literature on combustion is insufficient for understanding the physical phenomena in a volume that is comparable to a laminar flame thickness. Intensive theoretical and numerical efforts have been underway to face the new challenges [5, 6]. However, these models require benchmark data for assessments. Therefore, experimental measurements of pressure, velocity, temperature and reactive scalars either inside the microreactor or at the exit of microreactor are needed not only to gain a better insight into the physics but also to provide information for the input and validation of theoretical models. For the study of micro combustor, simultaneous measurement of temperature and multi-species concentration is a desirable feature for the measurement system. In hydrocarbon-fueled combustion systems, CO is one of the major combustion-generated pollutants and is an important molecule for combustion control purposes. CO_2 and H_2O are the major products that can provide information about the extent of combustion or mixing in a combustor and may be

used to improve fuel efficiency. CH_4 is the main constituent of natural gas and represents a pollutant in its unburned form. Moreover, CH_4 and O_2 are the key combustion parameters closely linked to the process stoichiometry. Therefore, simultaneous detections of multiple species and gas temperature using diode-laser based absorption spectroscopy not only allow a better understanding of the reacting flowfields but also provide information for adaptive, real-time combustion control [7].

Diode-laser sensor systems based on high-resolution absorption spectroscopy offer the potential of providing non-intrusive, absolute measurements of multiple flow parameters. Semiconductor diode lasers are attractive light sources for practical applications owing to their compactness, robustness, relatively inexpensive, and easy to use. In addition, these lasers are fiber-optic compatible and thus enable simultaneous measurements of multi-species and flow parameters along a common line of sight, by using time-division or wavelength-division multiplexing techniques. Diode-laser-based absorption spectroscopy techniques with commercially available room-temperature sources have been used for monitoring of O_2 [8, 9], CO [9-12], CO_2 [9-12], H_2O [9], and CH_4 [12-14] in a variety of sample gas cells. Recently, *in situ* measurements of O_2 [15], H_2O [16-19], CO_2 [20-22], CO [20, 22], and CH_4 [16] in flames or reaction chambers were reported. Simultaneous detection of multiple species has also been demonstrated by using various types of multiplexing techniques [11, 23]. Also, the gasdynamic parameters of flowfields, such as temperature, pressure, velocity, and mass flux, have been measured by use of the variations in intensity, line shape, and Doppler shift of these absorption spectra [15-19].

The past studies indicated that the measured flowfield parameters were obtained from comparisons of theoretical absorption spectra with experimental data. Therefore, an accurate prediction of species absorption spectra is essential for extracting valuable information from experimental measurements. This motivates the present study to theoretically study the absorption spectra of CO_2, CO, O_2, H_2O, and CH_4 in the near-IR region that can be used for future species concentration measurements. It should be noted that the focus of the present study is to accurately calculate the absorption spectra under known species mole fraction, temperature, and total pressure conditions. In practical applications of the absorption techniques to atmospheric flame measurements, the temperature must be determined first such that the mole fraction of a given species can be deduced from the measured line intensity and temperature.

4. Theory

The fundamental theory governing absorption spectroscopy is described by the Beer-Lambert law,

$$\frac{I}{I_o} = exp(-k_\nu L) \tag{1}$$

The ratio of the transmitted intensity I and initial (reference) intensity I_o of laser radiation through an absorbing medium at a particular frequency is exponentially related to the spectral absorption coefficient k_ν (cm^{-1}) and the absorption pathlength L [cm]. The spectral absorption coefficient k_ν is related to the total pressure P [atm], mole fraction of the absorbing species x_j, transition linestrength S_i [$cm^{-2}atm^{-1}$], and lineshape function $g(\nu - \nu_{0,i})$ [cm] by summing over all the rotational lines that contribute to the absorption in a particular wavelength region.

$$k_\nu = \sum_{i=1}^{N} P X_j S_i(T) g(\nu - \nu_{0,i}) \tag{2}$$

The species mole fraction can be obtained from the measured absorbance with known temperature and total pressure and related to the transition parameters by

$$X_j = \frac{-ln(I/I_0)}{PL\sum_{i=1}^{N} S_i(T) g(\nu - \nu_{0,i})} \tag{3}$$

The lineshape function describes the effects of broadening from thermal motion (Doppler broadening) and intermolecular collisions (collisional or pressure broadening). Doppler broadening is quantified through the Doppler width, $\Delta\nu_D$ which is the absorption line's full-width at half-maximum (FWHM) in the Doppler limit:

$$\Delta\nu_D = 7.1623\times10^{-7}\left(\frac{T}{m}\right)^{1/2}\nu_0 \tag{4}$$

where T is the temperature in Kelvin, m is the molecular mass in atomic mass units, and ν_0 is the line center transition frequency. Collisional broadening is described by a Lorentzian distribution:

$$g_L(\nu) = \frac{1}{2\pi}\frac{\Delta\nu_C}{(\nu-\nu_0)^2 + \left(\frac{\Delta\nu_C}{2}\right)^2} \tag{5}$$

where $\Delta\nu_C$ is the FWHM resulting from collisions and is termed the collision width. The collision width at a given temperature is directly proportional to pressure.

$$\Delta\nu_C = P\sum_A 2\gamma_A X_A \tag{6}$$

where P is the total pressure, γ_A is the broadening coefficient of the A^{th} perturber, and X_A is the mole fraction of the A^{th} component. The broadening coefficient's temperature variation is often modeled according to the following expression:

$$2\gamma(T) = 2\gamma(T_0)\left(\frac{T_0}{T}\right)^n \tag{7}$$

where T_0 is the reference temperature, $2\gamma(T_0)$ is the broadening coefficient at the reference temperature, and n is the temperature coefficient. Because n is typically less 1, collisional broadening decreases for increasing temperatures. At moderate pressures, the true lineshape is a convolution of the Doppler and collisional distributions, yielding a Voigt profile.

$$g(v) = 2\sqrt{\frac{ln\,2}{\pi}}\frac{V(a,x)}{\Delta v_D} \tag{8}$$

where $V(a, x)$ is the Voigt profile given by

$$V(a,x) = \frac{a}{\pi}\int_{-\infty}^{\infty}\frac{e^{-y^2}}{a^2+(x-y)^2}dy \tag{9}$$

a and x are defined as

$$a = \sqrt{ln\,2}\frac{\Delta v_C}{\Delta v_D} \tag{10}$$

$$x = \sqrt{ln\,2}\frac{(v-v_0)}{\Delta v_D} \tag{11}$$

When the Voigt parameter, a, is such that $0 < a < 1$, the Voigt profile becomes Gaussian shaped representative of Doppler broadening being predominant. As pressure increases and, thus a, the Voigt profile begins developing broad wings and when the Voigt parameter reaches 2, the profile is primarily Lorentzian.

The linestrength as a function of temperature for a particular transition i is governed by its linestrength S_i at a reference temperature T_0, the partition function $Q(T)$, the frequency of the transition $v_{0,i}$, and the lower-state energy of the transition E_i''. The relationship is given by

$$S_i(T) = S_i(T_0)\frac{Q(T_0)}{Q(T)}\left(\frac{T_0}{T}\right)exp\left[-\frac{hcE_i''}{k}\left(\frac{1}{T}-\frac{1}{T_0}\right)\right]$$
$$\times\left[1-exp\left(\frac{-hcv_{0,i}}{kT}\right)\right]\left[1-exp\left(\frac{-hcv_{0,i}}{kT_0}\right)\right]^{-1} \tag{12}$$

The partition function can be calculated by classical means as a product of the rotational and vibrational partition functions, Q_{rot} and Q_{vib}, respectively. With the rigid-rotator model, the rotation partition function for diatomic molecules can be calculated as

$$Q_{rot} = \frac{T}{\sigma T_r} \tag{13}$$

in which $\sigma = 1$ for heteronuclear molecules, $\sigma = 2$ for homonuclear molecules, and T_r is the characteristic rotational temperature. For non-linear polyatomic molecules, the relation for Q_{rot} is

$$Q_{rot} = \frac{8\pi^2}{\sigma h^3}\left(I_x I_y I_z\right)^{1/2}\left(2\pi kT\right)^{3/2} \tag{14}$$

where I_x, I_y, and I_z are the three principal moments of inertia, h is Planck constant, and k is Boltzmann constant. With the simple harmonic oscillator model, the vibrational partition function can be represented by [24]

$$Q_{vib} = \left[1-exp\left(\frac{-hcv_1}{kT}\right)\right]^{-d_1}\left[1-exp\left(\frac{-hcv_2}{kT_0}\right)\right]^{-d_2}$$
$$\left[1-exp\left(\frac{-hcv_3}{kT}\right)\right]^{-d_3}\ \ldots\ldots \tag{15}$$

where d_1, d_2, d_3, …are the degrees of degeneracy of the vibrational frequencies v_1, v_2, v_3, …, respectively.

5. Results and Discussion

5.1 Line Selection

Figure 1 illustrates the near-IR line strengths of CO_2, CO, H_2O, and CH_4 over a range of wavelengths from 1 to 2 μm and of O_2 from 0.5 to 1.5 μm at a temperature of 296 K [25]. The vertical dashed lines denote those wavelengths that have been used for absorption measurements. As shown in Figure 1, H_2O is a relatively strong absorber throughout the near-IR region, while CO_2, CO, O_2, and CH_4 have weaker but distinct absorption bands. Although H_2O has strong infrared signature and makes it an attractive target species for *in situ* temperature measurement, it also provides significant spectral interference for measurements of other species. In order to avoid strong H_2O spectral interference, previous measurements have been made by probing the relatively weak overtone and combination bands of CO and CO_2 near 1.55 μm [9-15], CH_4 near 1.65 μm [12-14], and O_2 near 0.76 μm [8, 9]. Measurement of H_2O near 1.79 μm has demonstrated its absorption spectrum free of interference from CH_4 [9]. In addition, H_2O transitions near 1.31 μm [17] and 1.34 and 1.39 μm [18] were demonstrated as a candidate wavelength for species concentration and temperature measurements. The surveyed spectra indicate that the linestrengths increase with increasing wavelength towards 2.0 μm or higher, especially for CO_2 and H_2O. However, a diode-laser with output wavelength higher than 2.0 μm is still relatively expansive and unstable. Therefore, the present study is aimed to simulate the absorption spectra

below 2.0 μm and to valid the predictions with existing experimental data.

5.2 Theoretical Spectra

The accurate predictions of absorption spectra strongly rely on the fundamental spectroscopic parameters, including linestrength, lower-state energy, broadening coefficients, lineshape function, and partition function. The linestrength, lower-state energy, and broadening coefficients can be obtained from HITRAN 96 database [25]. The lineshape and partition functions then have to be calculated through Equations (4)-(11) and (13)-(15). An accurate value of the partition function is required for determining the line strengths at temperatures other than the reference temperature. Figure 2 shows the calculated partition functions for CO_2, CO, O_2, H_2O, and CH_4 over a range of temperature from 300 to 1500 K. It is noted that the partition function of CO_2 calculated from classical model is the same as that approximated using a third-order polynomial fit of HITRAN 96 data [25]. Figure 2 indicates that the partition functions increase exponentially with temperature. This implies that the linestrength of a probed species would generally become weaker as temperature is increased.

5.2.1 CO_2 Absorption Spectra

The calculated short-scanning spectrum of the CO_2 $2\nu_1 + 2\nu_2^0 + \nu_3$ band (R branch) is compared with the measured data obtained from 296 K, 338-Toor total pressure, 3276-cm absorption path length, and a mixture of 8.31% CO_2 in air [12] as shown in Figure 3. The agreement between the calculated and measured data is good for low rotational level up to $J'' = 10$. For higher rotational quantum numbers ($10 < J'' < 34$), the calculation overpredicts the measured absorbance by as much as 15%. The calculated spectrum is also in good agreement with that calculated by Mihalcea et al. [12]. Figure 4 shows comparison of the calculated two-line Voigt fit spectrum of the CO_2 $R(16)$ and $R(4)$ transitions (near 6359.97 cm^{-1}) with the measured data recorded in a multiple path cell (X_{CO2} =7.56%, 297 K, 189 Torr, 3276-cm absorption path) from sampled combustion gases at $\phi = 1.27$ [12]. The agreement between the Voigt fit and the measured data is generally good. The effects of pressure on the broadening of absorption features are also shown in Figure 4a. It is noted that the pressure-induced line shift is not considered in the calculation. Figure 4b illustrates the Doppler effects on the absorption spectra due to increased temperature. It can be seen that the peak intensities of $R(16)$ decrease and of $R(4)$ increase with increasing temperatures. This suggests that the ratio of two peak intensities may be used for simultaneous gas temperature and CO_2 concentration measurements. A simulation of CO_2 absorption lineshape at flame condition is also performed and compared with the measured data as shown in Figure 5. The experimental data are measured in the combustion region of a premixed ethylene-air flame by use of the $R(50)$ transition near 2 μm with $\phi = 0.79$, $X_{CO2} = 0.105$, $T = 1690$ K, $P = 1$ atm, and $L = 17$ cm [21]. Figure 5 shows that the calculation with single-line Voigt fit ($a = 1.32$) satisfactorily reproduce the experimental data.

5.2.2 CO and O_2 Absorption Spectra

Figure 6 shows the comparison of the calculated single $R(13)$ transition of CO (X_{CO} = 2.18%) with the experimental data obtained from sampling combustion gases at $\phi = 1.08$ and measured at cell conditions of 297 K and 239 Torr over an absorption length of 3276 cm [12]. The agreement between the best-fit Voigt profile and the data is good.

Comparison of the calculated O_2 $PQ(11, 10)$ transitional spectra in laboratory air with the measured data [21] is shown in Figure 7. It can be seen that the calculation using collisional coefficients from HITRAN96 results in a slightly broader line width, while adapting the Voigt parameter ($a = 2.47$) used in [21] matches the measured profile.

5.2.3 H_2O Absorption Spectra

Figure 8 shows the comparison of calculated and measured spectral feature of H_2O in a 0.2 cm^{-1} spectral window near 5567.75 cm^{-1} (297 K, 114 Torr, 1.15% H_2O in air) [9]. The spectra shown in Figure 8a is calculated using HITRAN96 database. The spectral feature is a convolution of two-line Voigt fit. It can be seen that the measured spectrum [9] (Figure 8b) is slightly different from the one predicted using HITRAN96 database (Figure 8a). The measurements indicate that the actual spectral separation between the overlapping lineshapes is 0.23 cm^{-1} and not 0.011 cm^{-1} as tabulated in HITRAN96. The calculated spectrum using measured frequencies and two-line Voigt fit of profiles compares well with experimental data.

5.2.4 CH_4 Absorption Spectrum

Figure 9 shows the calculated and measured absorbance of the $R(6)$ manifold of CH_4 ($2\nu_3$) near 1.645 μm, recorded in a cell at 295 K, 5.0 Torr, $X_{CH4} = 1.0$, and a 40-cm absorption path length [13]. The calculated contributions from the individual rotational lines are depicted by broken curves.

The best match of the experimental data is obtained from a convolution of six-line Voigt profiles. In general, for cases with significant collisional broadening, the measured over-lapping line should be modeled with multiple profiles with individual Voigt *a* parameters [13]. However, for such a low pressure condition (P = 5.0 Torr), the contributions of collisional broadening to the Voigt *a* parameters are small compared to Doppler broadening. Therefore, the Voigt profile is represented by Doppler profile.

Recently, absorption measurements of spectroscopic parameters in the $R(3)$ and $R(4)$ manifolds of $2\nu_3$ band of CH_4 at elevated temperatures have been reported [14]. Therefore, we also perform the calculations of these two manifolds to assess the capability of predicting CH_4 absorption spectra at elevated temperatures. Comparisons of the calculated and measured absorption features for the $R(3)$ and $R(4)$ transitions at room and high temperature are shown in Figures 10 and 11, respectively. It can be seen that the $R(3)$ and $R(4)$ manifolds consist of three and four individual line contributions, respectively. The best fits to the experimental data are obtained by a convolution of multiple linestrengths. Comparison of Figures 10 and 11 indicate that the effects of collisional broadening and Doppler broadening on the spectra become significant as the pressure and temperature are increased. These effects result in a broader lineshape and a decreased absorbance. Nevertheless, the present study demonstrates that the absorption features of a non-linear polyatomic molecule such as methane can be accurately predicted.

5.2.5 Experimental Results

Figure 12 shows the experimental setup consisting of a test cell and the diode laser system. The light source is a L-band tunable diode laser with a wavelength tuning range of 1.566-1.607 μm, a tuning step size of 25 GHz (0.833 cm^{-1}), a tuning speed of 1.2 s, and an output power of 10 mW. The laser output is split into two beams with single-mode 1 × 2 fiber splitter. One output from the splitter is used to measure reference intensity, I_0. The other output is directed into the test cell and focus at exit onto a detector to measure the transmitted intensity, I. InGaAs detectors are used to measure the output signals.

Experimental measurement of CO_2 absorption spectrum is obtained by scanning the diode laser from 6220 to 6385 cm^{-1}. The test cell is filled with CO_2 and operated at T = 296 K and P = 1 atm. Comparison of the measured and calculated CO_2 spectra is illustrated in Figure 13. Figure 13a shows the calculated absorption spectrum by assuming a narrow laser linewidth of 0.001 cm^{-1}. It can be seen that the rotational lines are well separated if the laser linewidth is narrow. However, if the laser linewidth (0.8 cm^{-1}) is broad, the absorption lines become overlapped, as shown in Figure 13b. It is noted that the mismatched peak positions of the measured and calculated spectra may be due to large scanning step of the laser and incorrect interpretation of the output signals. This requires further investigations.

6. Conclusions

Theoretical study of CO_2, CO, O_2, H_2O, and CH_4 absorption spectra under various pressure and temperature conditions are made to assess the developed numerical codes by comparing the predictions with existing experimental data. Results indicate that an accurate calculation of the partition function and line shape function is essential for extracting species mole fraction from the absorption measurements. It is found that a single Voigt fit to the lineshape can be used for linear molecules (CO_2, CO, and O_2), while the non-linear molecules (H_2O and CH_4) require a convolution of multiple Voigt profiles due to closely spaced multiple transition lines. It should be noted that the gases investigated in the present theoretical study are either pure or extracting from the flame into a relatively low pressure test cell. Therefore, further improvements of the model to account for multi-perturber collision, aerosol extinction, optical window transmission, beam-steering, and pressure-induced frequency shift effects are warranted because our final goal is to develop diode-laser based sensors for species concentrations and gas temperature measurements in hostile combustion environments.

7. Self Evaluation

In this project, a numerical code has been developed for theoretical predictions of absorption spectra of combustion products in the near infrared region. The capability of the code has been demonstrated by comparing the predicted absorption spectra with reported experimental data. However, the code still needs further improvement so that it can be applied to real combustion environments. In addition, due to the shortage of the funding instrumentation budget (NT$ 320K), the linewidth and scanning step of the purchased telecommunication diode laser is much poorer than those (NT$ 1500K) used by Prof. Hanson's group at Stanford University. Therefore, the sufficient instrumentation budget is essential to achieve the world's research level.

8. References

[1] G. T. A. Kovacs, (1998) *Micromachined transducers-source book*. New York, McGraw-Hill.

[2] K. Maruta, K. Takeda, L. Sitzki, K. Borer, P. D. Ronney, S. Wussow, and O. Deutschmann, (2001) Catalytic Combustion in Microchannel for MEMS Power Generation. Third Asia-Pacific Conference on Combustion, Seoul, Korea, June 24–27.

[3] A. H. Epstein et al., (1997) Micro-heat engines, gas turbines, and rocket engines. AIAA 97-1773, presented at 28th AIAA Fluid Dynamics Conference, 4th AIAA Shear Flow Control Conference, June29-July 2, Snowmass Village, CO.

[4] A. C. Fernandez-Pello, (2002) Micropower Generation Using Combustion: Issues and Approaches. *Proceedings of the Combustion Institute*, Volume 29, pp. 883–899.

[5] D. H. Lee and S. Kwon, (2002) Heat transfer and quenching analysis of combustion in a micro combustion vessel. *J. Micromech. Microeng*. **12**, 670-676.

[6] E. S. Oran, C. K. Oh and Z. C. Cybyk, (1998) Direct simulation Monte Carlo: recent advances and applications. *Annu. Rev. Fluid Mech*. **30**, 403-441.

[7] Furlong, E. R., Baer, D. S., and Hanson, R. K., "Real-Time Adaptive Combustion Control Using Diode-Laser Absorption Sensors," *Proceedings of the Combustion Institute,* Vol. **27**, 1998, pp. 335-342.

[8] Nguyen, Q. V., Dibble, R. W., and Day, T., "High-Resolution Oxygen Absorption Spectrum Obtained With an External-Cavity Continuously Tunable Diode Laser," *Opt. Lett.*, Vol. **19**, 1994, pp. 2134–2136.

[9] Mihalcea, R. M., Baer, D. S., and Hanson, R. K., "A Diode-Laser Absorption Sensor System for Combustion Emission Measurements," *Meas. Sci. Technol.*, Vol. **9**, 1998, pp. 327–338.

[10] Sonnenfroh, D. M. and Allen, M. G., "Observation of CO and CO2 Absorption near 1.57 μm With an External-Cavity Diode Laser," *Appl. Opt.*, Vol. **36**, 1997, pp. 3298–3300.

[11] Oh, D. B., Paige, M. E., and Bomse, D. S., "Frequency Modulation Multiplexing for Simultaneous Detection of Multiple Gases by Use of Wavelength Modulation Spectroscopy with Diode Lasers," *Appl. Opt.*, Vol. **37**, 1998, pp. 2499–2501.

[12] Mihalcea, R. M., Baer, D. S., and Hanson, R. K., "Diode-Laser Sensor System for Measurements of CO, CO_2, and CH_4 in Combustion Flows," *Appl. Opt.*, Vol. **36**, 1997, pp. 8745–8752.

[13] Nagali, V., Chou, S. I., Baer, D. S., and Hanson, R. K., "Tunable Diode-Laser Absorption Measurements of Methane at Elevated Temperatures," *Appl. Opt*., Vol. **35**, 1996, pp. 4026–4032.

[14] Gharavi, M. and Buckley, S. G., "Diode Laser Absorption Spectroscopy Measurement of Linestrengths and Pressure Broadening Coefficients of the Methane $2\nu_3$ Band at Elevated Temperatures," *J. Molecular Spectroscopy*, Vol. 229, 2005, pp. 78-88.

[15] Miller, M. F., Kessler, W. J., and Allen, M. G., "Diode Laser-Based Air Mass Flux Sensor for Subsonic Aeropropulsion Inlets," *Appl. Opt.*, Vol. **35**, 1996, pp. 4905–4912.

[16] Silver, J. A., Kane, D. J., and Greenberg, P. S., "Quantitative Species Measurements in Microgravity Flames With Near-IR Diode Lasers," *Appl. Opt.*, Vol. **34**, 1995, pp. 2787–2801.

[17] Allen, M. G. and Kessler, W. J., "Simultaneous Water Vapor Concentration and Temperature Measurements Using 1.31 μm Diode Lasers," *AIAA J.*, Vol. **34**, 1996, pp. 483–488.

[18] Baer, D. S., Nagali, V., Furlong, E. R., Hanson, R. K., and Newfield, M. E., "Scanned- and Fixed-Wavelength Absorption Diagnostics for Combustion Measurements Using Multiplexed Diode Lasers," *AIAA J.*, Vol. **34**, 1996, pp. 489–493.

[19] Mihalcea, R. M., Baer, D. S., and Hanson, R. K., "Advanced Diode Laser Absorption Sensor for *in-situ* Combustion Measurements of CO2, H2O, and Gas Temperature," AIAA Paper 98-0237, 1998.

[20] Sonnenfroh, D. M. and Allen, M. G., "Diode Laser Sensors for Combustor and Aeroengine Emission Testing: Applications to CO, CO2, OH, and NO," AIAA Paper 96-2226, 1996.

[21] Webber, M. E., Kim, S., Sanders, S. T., Baer, D. S., Hanson, R. K., and Ikeda, Y., "I*n-Situ* Combustion Measurements of CO_2 by Use of a Distributed-Feedback Diode-Laser Sensor Near 2.0 μm," *Appl. Opt*., Vol. 40, 2001, pp. 821-828.

[22] Ebert, V., Teichert, H., Strauch, P., Kolb, T. Seifert, H., and Wolfrum, J., "Sensitive In Situ Detection of CO and CO_2 in a Rotary Kiln Based Hazardous Waste Incinerator Using 760 nm and New 2.3 μm Diode Lasers," *Proceedings of the Combustion Institute*, Vol. **30**, 2005, pp. 1611-1618.

[23] Baer, D. S., Hanson, R. K., Newfield, M. E., and Gopaul, N. K. L. M., "Multiplexed Diode-Laser Sensor System for Simultaneous H2O, O2, and Temperature Measurements," Opt. Lett., Vol. **19**, 1994, pp. 1900–1902.

[24] Herzberg, G., *Molecular Spectra and Molecular Structure II. Infrared and Raman Spectra of Polyatomic Molecules.* Van Nostrand, New York, 1960.

[25] Rothman, L. S., Rinsland, C. P., Goldman, A., Massie, S. T., Edwards, D. P., Flaud, J. M., Perrin, A., Camy-Peyret, C., Dana, V., Mandin, J.-Y., Schroeder, J., McCann, A., Gamache, R. R., Wattson, R. B. , Yoshino, K., Chance, K. V., Jucks, K. W., Brown, L. R., Nemtchinov, V., and Varanasi, P., "The HITRAN molecular spectroscopic database and HAWKS (HITRAN atmospheric workstation): 1996 edition," *J. Quant. Spectrosc. Radiat. Transfer*, Vol. **60,** 1998, pp. 665–710.

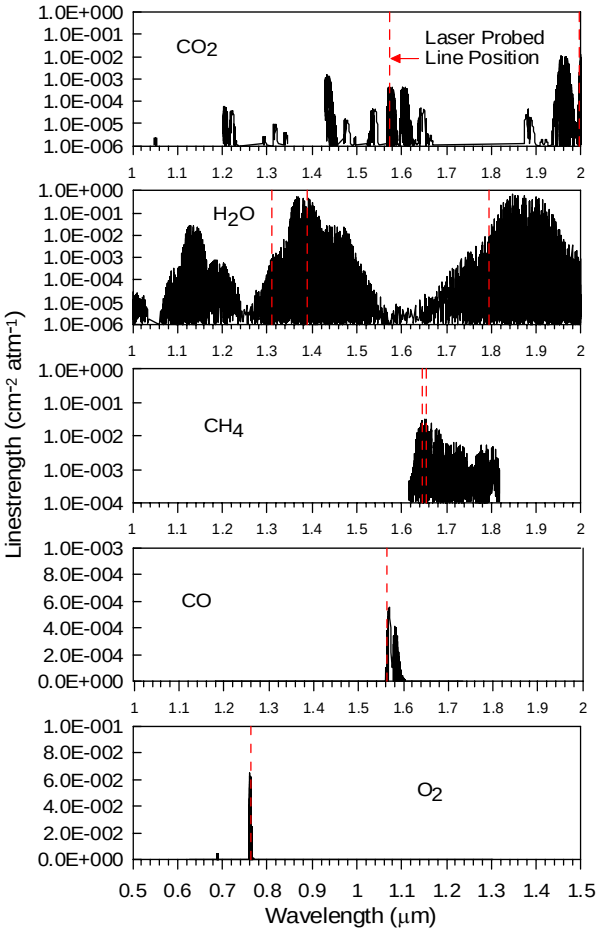

Figure 1 Linestrengths of CO_2, CO, H_2O, and CH_4 in the 1 to 2 μm and of O_2 from 0.5 to 1.5 μm at a temperature of 296 K (from HITRAN 96 database [19]).

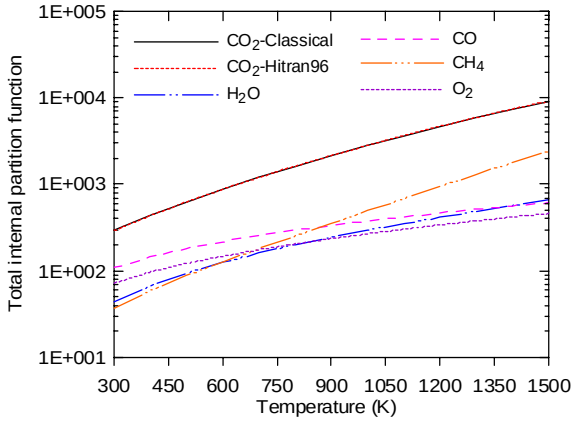

Figure 2 The calculated partition functions for a range of temperature from 300 to 1500 K.

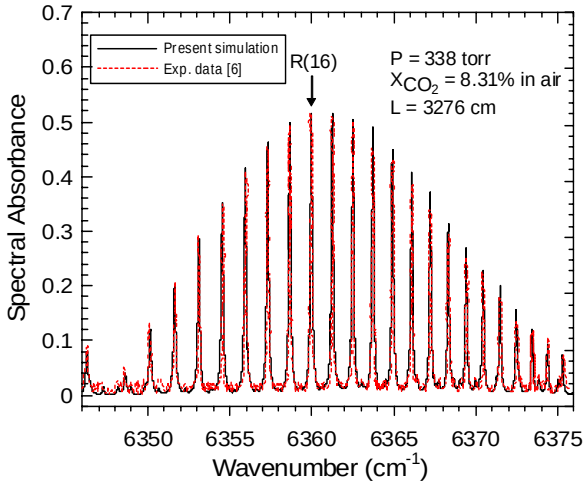

Figure 3 Comparison of the calculated and measured spectral absorbance of the CO_2 *R*-branch.

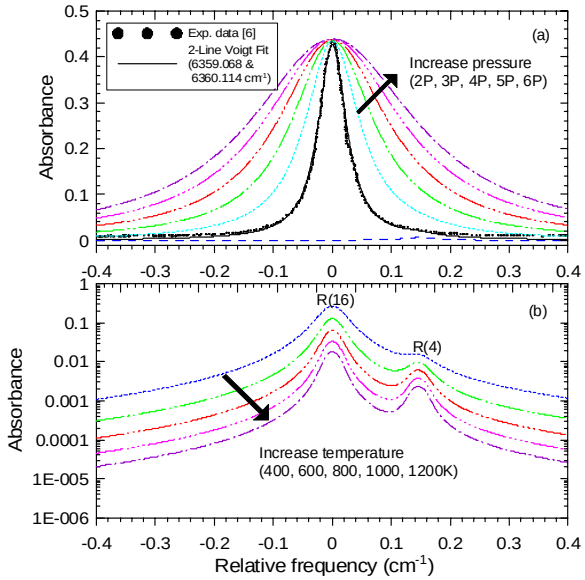

Figure 4 Comparison of the calculated and measured spectral absorbance of the CO_2 *R*(16) rotational line. (a) Effects of pressure on the spectra, (b) Effects of temperature on the spectra.

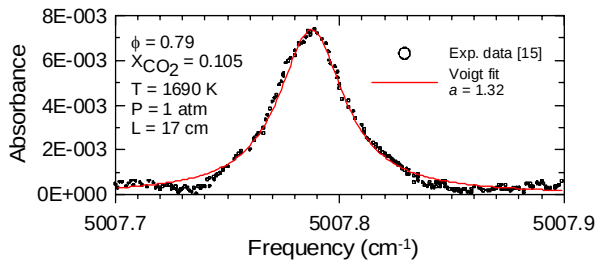

Figure 5 Comparison of the calculated and measured spectral absorbance of the CO_2 $R(50)$ rotational line.

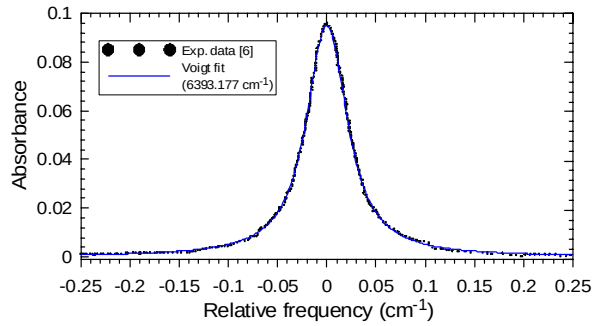

Figure 6 Comparison of the calculated and measured spectral absorbance of the CO $R(13)$ rotational line.

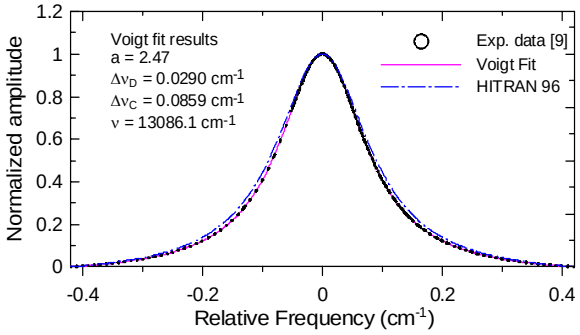

Figure 7 Comparison of the calculated and measured lineshapes of the O_2 $PQ(11, 10)$ transition at 13086.1 cm^{-1}.

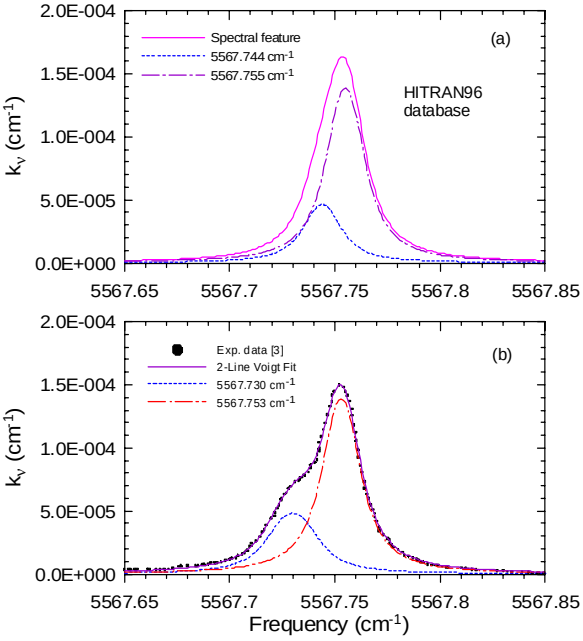

Figure 8 Comparison of the calculated and measured spectral absorption coefficient of H_2O near 5567.75 cm^{-1} (297 K, 114 Torr, 1.15% H_2O in air).

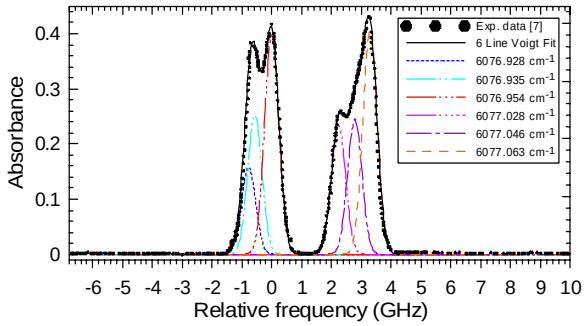

Figure 9 Comparison of the calculated and measured lineshapes of the $R(6)$ manifold of CH_4 near 1.645 μm recorded in a test cell at 295 K, 5.0 Torr, X_{CH4} = 100%, with a 40-cm absorption path length..

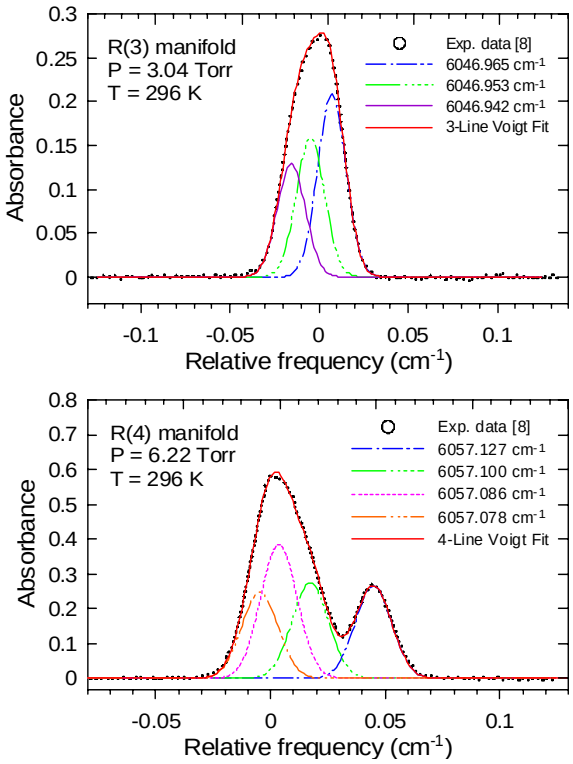

Figure 10 Comparison of the calculated and measured lineshapes of the *R*(3) manifold (upper trace)and *R*(4) manifold (lower trace) of CH_4 at 296 K.

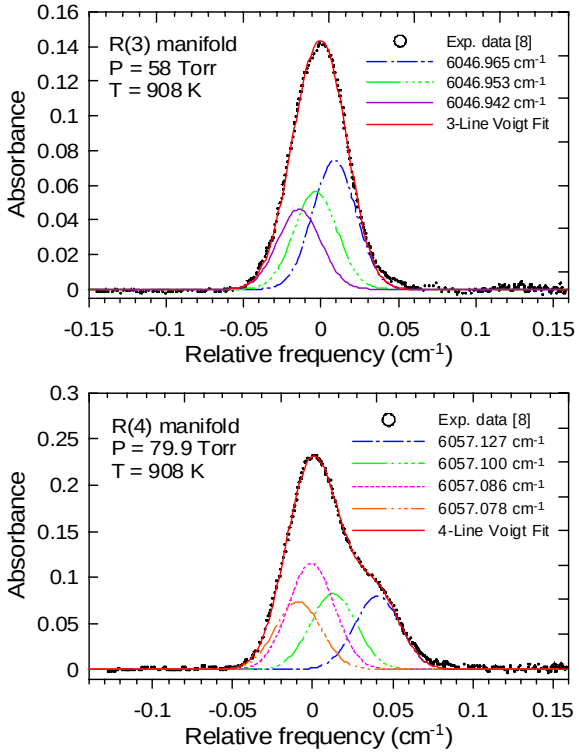

Figure 11 Comparison of the calculated and measured lineshapes of the *R*(3) manifold (upper trace)and *R*(4) manifold (lower trace) of CH_4 at 908 K.

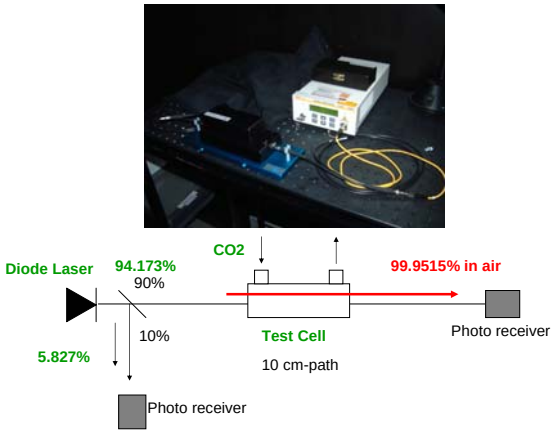

Figure 12 Experimental setup of the diode-laser sensor system.

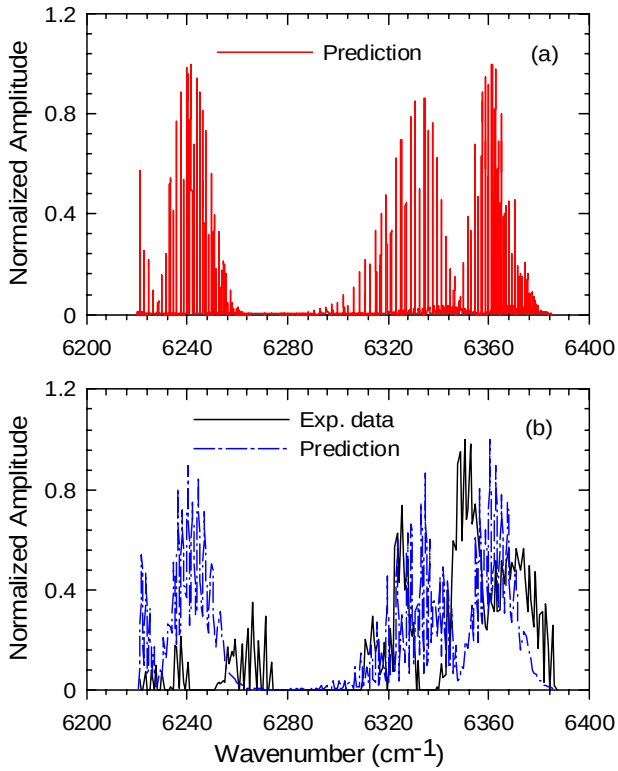

Figure 13 Comparison of measured and calculated CO_2 spectra. (a) Prediction with narrow laser linewidth ($\Delta\nu$ = 0.001 cm^{-1}), (b) Prediction with broad laser linewidth ($\Delta\nu$ = 0.8 cm^{-1}).